Electronic Supplementary Material (ESI) for Nanoscale.

SUPPLEMENTARY INFORMATION

Enhanced Li-ion storage performance of novel tube-in-tube structured nanofibers with hollow metal oxide nanospheres covered with a graphitic carbon layer

Gi Dae Park and Yun Chan Kang*

Department of Materials Science and Engineering, Korea University, Anam-Dong, Seongbuk-Gu, Seoul 136-713, Republic of Korea.

Experimetal Section

1. Materials characterization

The morphologies of nanofibers were investigated using scanning electron microscopy (SEM, VEGA3) and transmission electron microscopy (TEM, JEM-2100F). The crystal structures and chemical properties of nanofibers were analyzed using X-ray diffraction spectroscopy (XRD, X'pert PRO with Cu K_α radiation, $\lambda = 1.5418$ Å) at the Korea Basic Science Institute, Daegu, and X-ray photoelectron spectroscopy (XPS, Thermo Scientific™, K-Alpha™). The properties and the amount of pitch derived carbon was characterized via Raman spectroscopy (Jobin Yvon LabRam HR800), using a 632.8 nm He/Ne laser at room temperature for excitation, and thermogravimetric analysis (TGA, Pyris 1 Thermogravimetric Analyzer, PerkinElmer) in the range of 25–700 ^{o}C at 10 ^{o}C min^{-1} in an air-based atmosphere, respectively. The surface area and porosities of samples were analyzed using the Brunauer–Emmett–Teller (BET) method with high-purity N_2.

2. Electrochemical measurements

The electrochemical properties of the nanofibers were analyzed using a 2032-type coin cell. The anode was prepared by mixing the active material, carbon black, and sodium carboxymethyl cellulose in a weight ratio of 7:2:1. Lithium metal and microporous polypropylene films were used as counter electrode and separator, respectively. The electrolyte was 1 M $LiPF_6$ dissolved in a mixture of fluoroethylene carbonate−dimethyl carbonate (FEC/DMC; 1:1 v/v). The discharge and charge characteristics of the samples were investigated by cycling in the potential range of 0.001−3.0 V at various current densities. Cyclic voltammograms (CVs) were measured at a scan rate of 0.1 mV s^{-1}. Electrochemical impedance spectroscopy (EIS) was performed on the electrode over a frequency range of 0.01–100 kHz. In-situ EIS analysis was performed at preselected potentials during the discharge and charge processes at a current density of 0.1 A g^{-1}. For full cell assembly, yolk-shell structured $LiNi_{0.5}Mn_{1.5}O_4$ powders with a loading mass of 4.2 mg cm^{-2} were used as cathode, while the anode mass loading was maintained at 0.42 mg cm^{-2}. Further information on $LiNi_{0.5}Mn_{1.5}O_4$ powders has been provided in our previous reports. The electrolyte was a 1.0 M $LiPF_6$ dissolved in an ethylene carbonate/diethyl carbonate mixture (EC/DEC; 1:1 v/v). Before assembling the full cell, the anode was pretreated using electrochemical lithiation to suppress the first irreversible capacity loss. The electrochemical properties of the 2032-type coin full cells were examined at 0.5 A g^{-1} in the potential window of 2.0–4.6 V. The electrode capacity was calculated according to the weight of the anode materials.

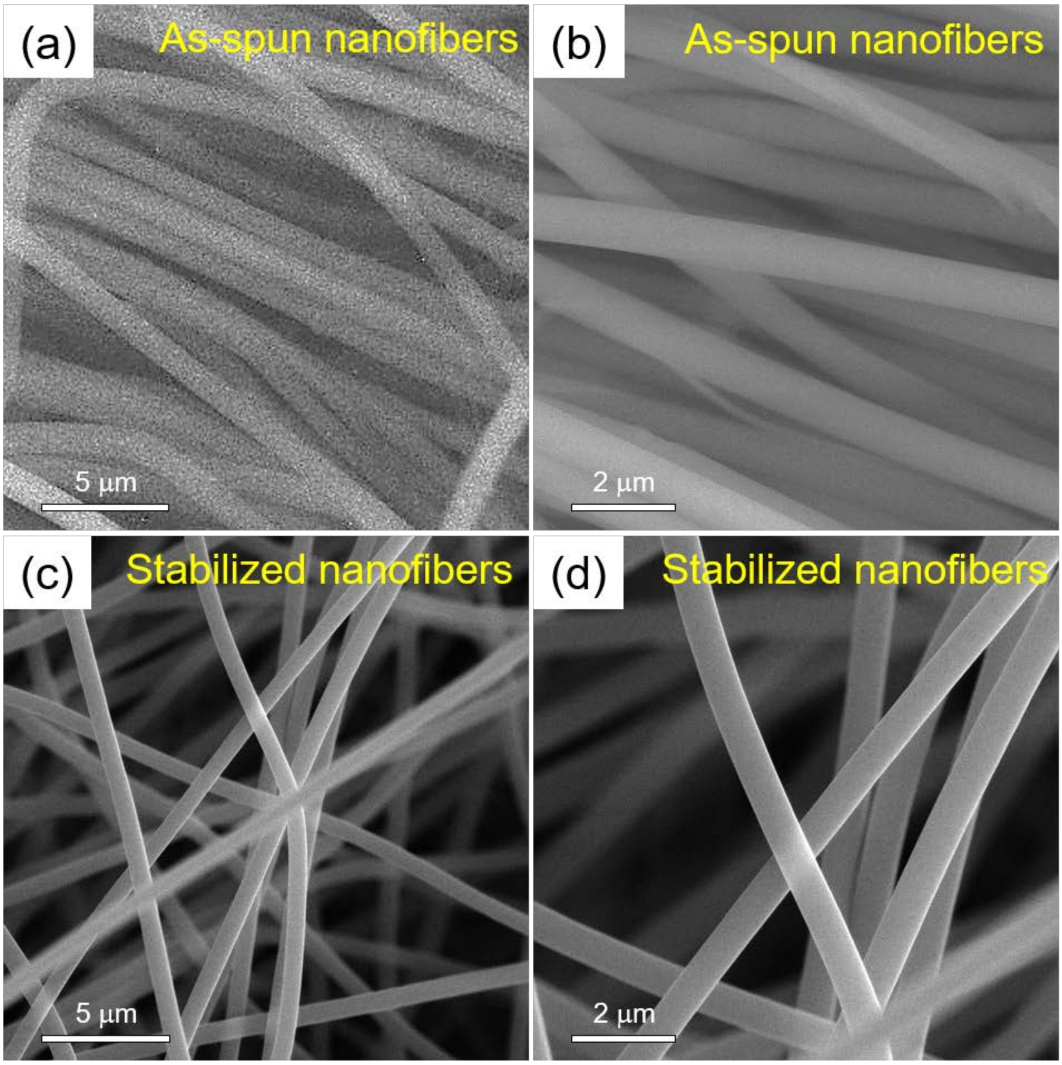

Fig. S1. Morphologies of of as-spun $Co(acac)_3$-$Fe(acac)_3$-PAN composite precursor nanofibers and stabilized nanofibers: (a,b) as-spun precursor nanofibers and (c,d) stabilized nanofibers.

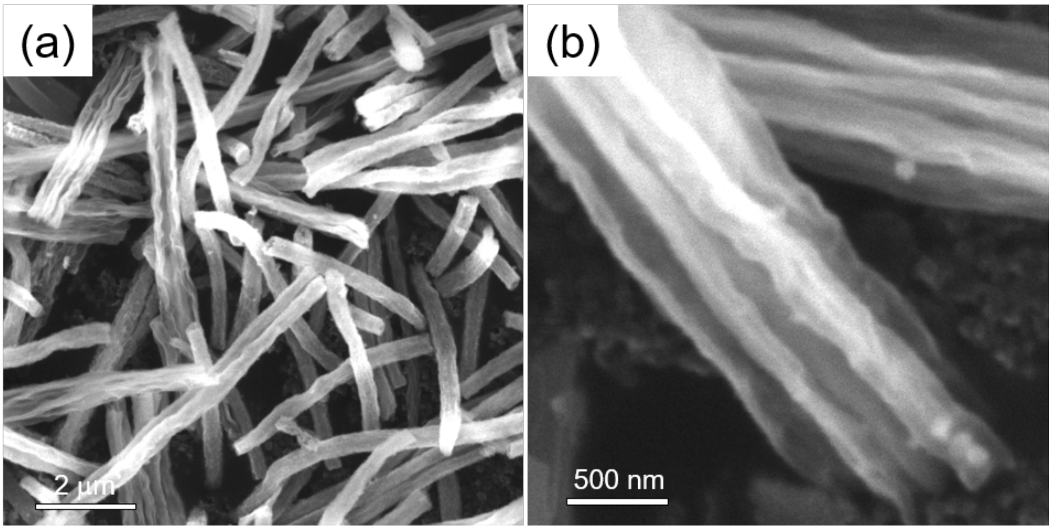

Fig. S2. Morphologies of $CoFe_2O_4$ nanofibers with tube-in-tube nanostructures ($CoFe_2O_4$_TIT).

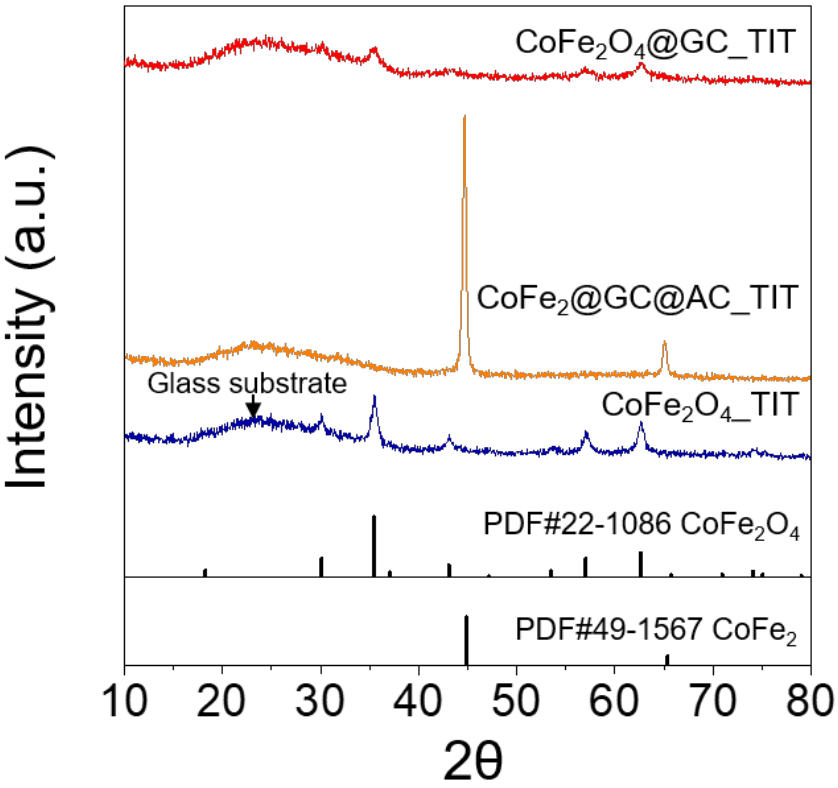

Fig. S3. XRD patterns of $CoFe_2O_4$_TIT, $CoFe_2$@GC@AC_TIT, and $CoFe_2O_4$@GC_TIT.

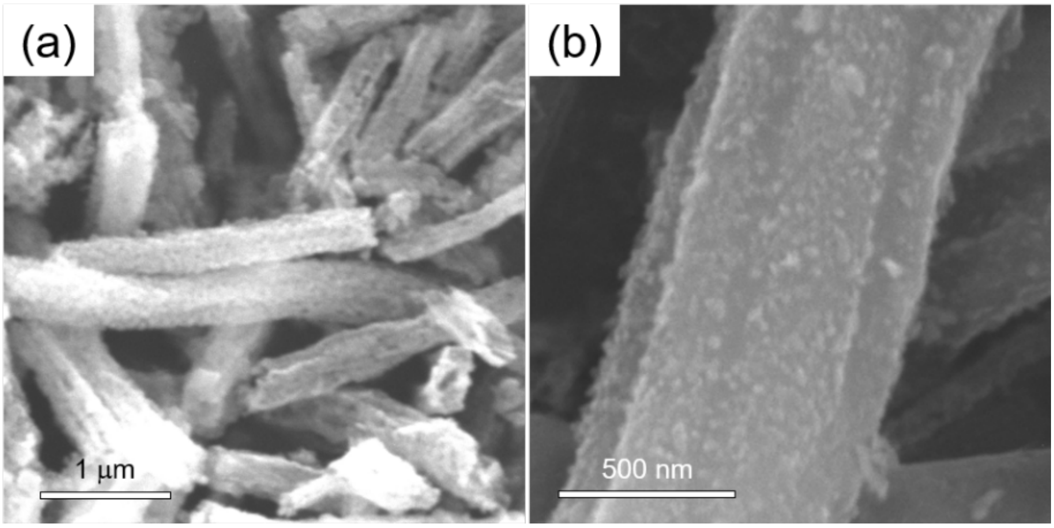

Fig. S4. Morphologies of $CoFe_2$@GC@AC nanofibers with tube-in-tube nanostructures ($CoFe_2$@GC@AC_TIT).

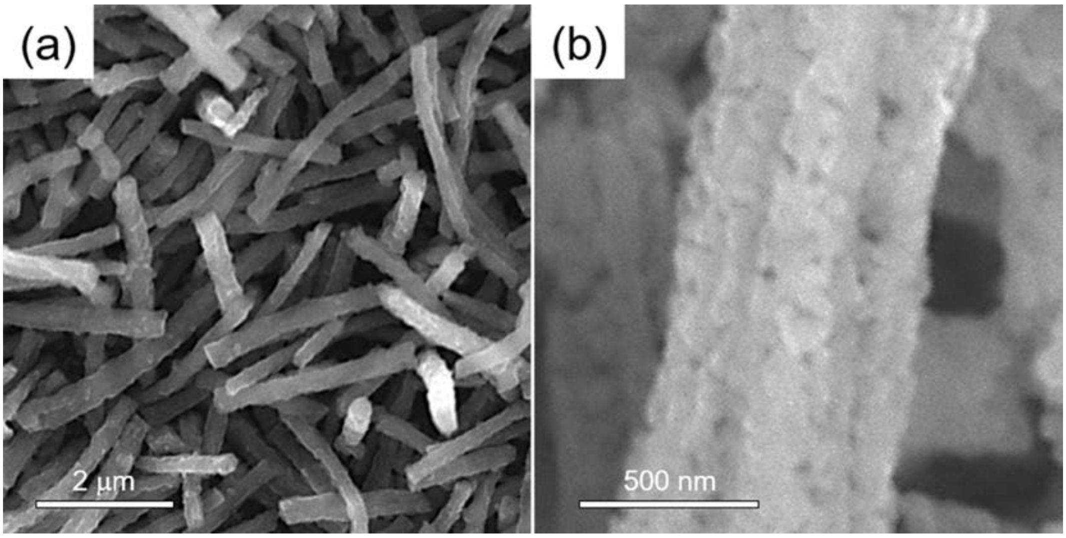

Fig. S5. Morphologies of tube-in-tube structured nanofibers comprising hollow $CoFe_2O_4$ nanospheres coated with GC layers ($CoFe_2O_4$@GC_TIT).

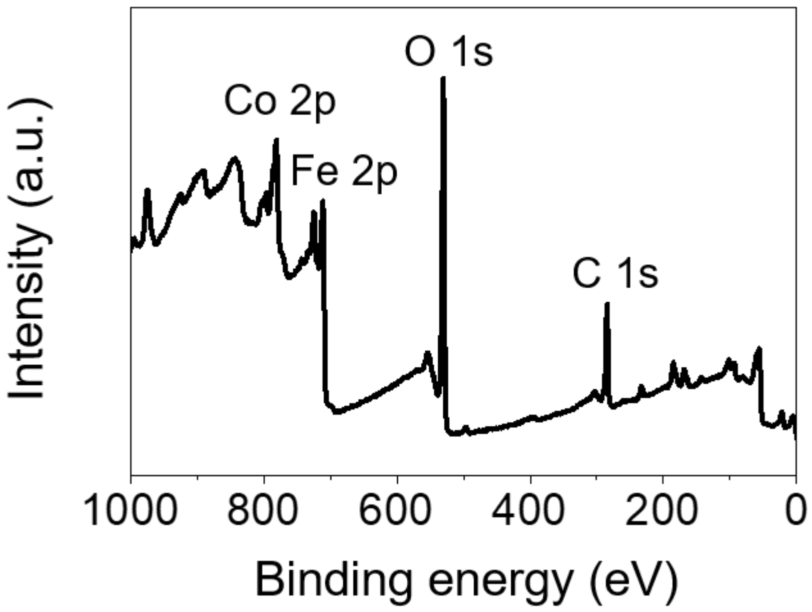

Fig. S6. XPS survey scan of $CoFe_2O_4$@GC_TIT.

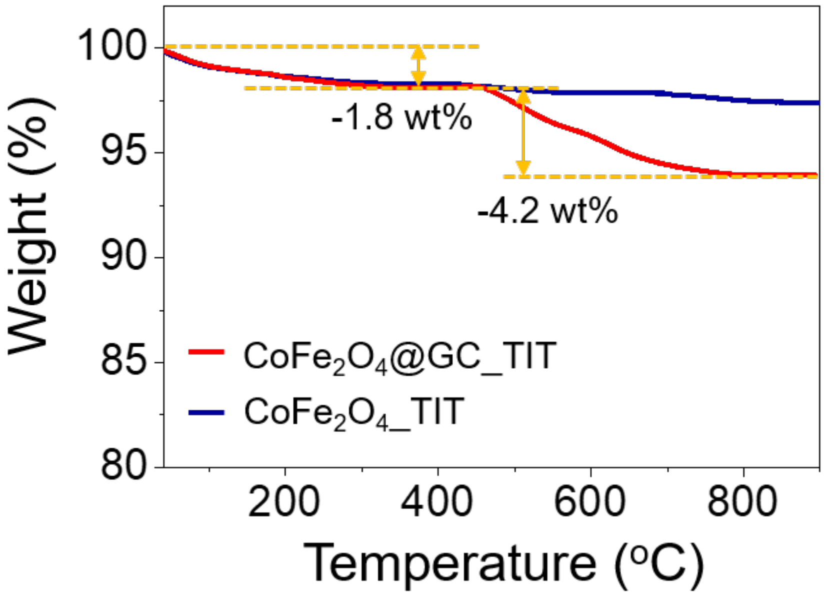

Fig. S7. TG curve of $CoFe_2O_4$@GC_TIT and $CoFe_2O_4$_TIT.

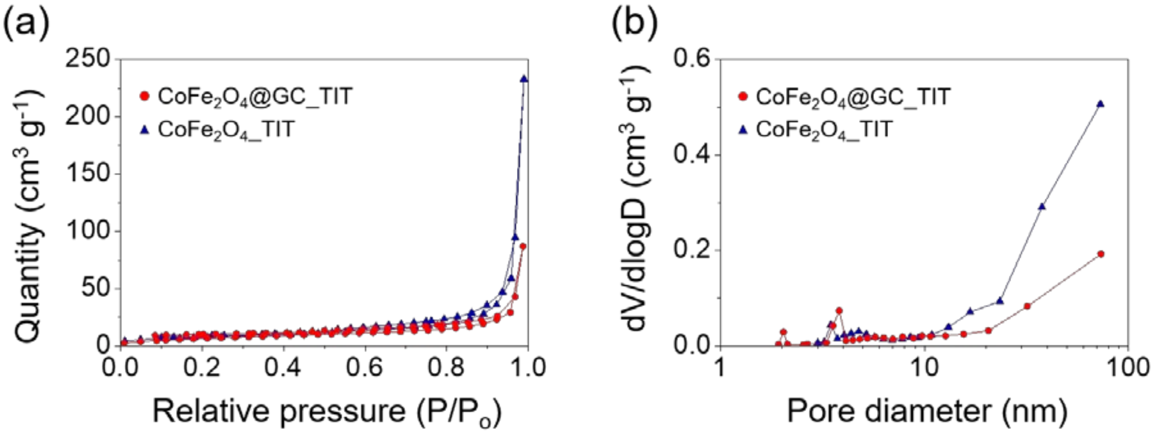

Fig. S8. (a) N_2 gas adsorption and desorption isotherms and (b) pore size distributions of $CoFe_2O_4$@GC_TIT and $CoFe_2O_4$_TIT.

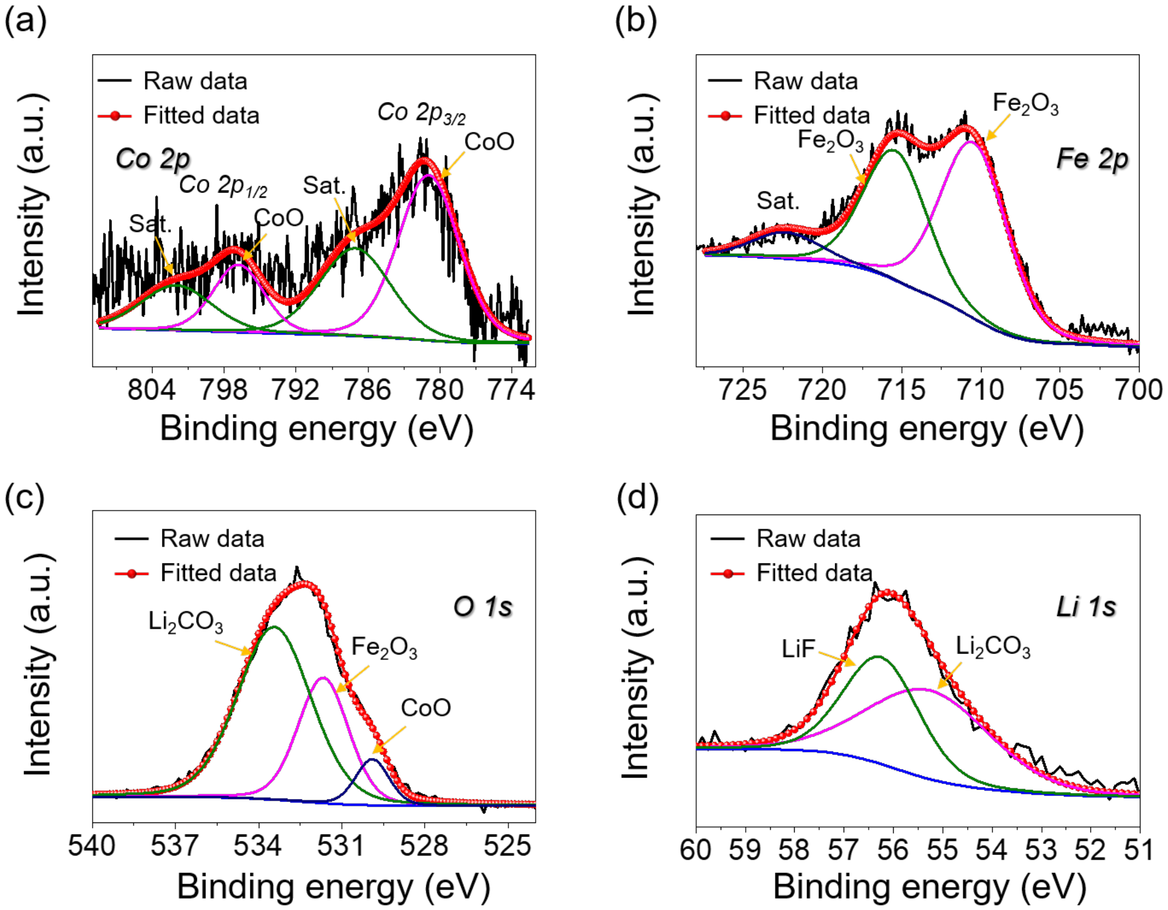

Fig. S9. XPS spectra of $CoFe_2O_4$@GC_TIT obtained after the first cycle: (a) Co 2p, (b) Fe 2p, (c) O1s, and (d) Li 1s.

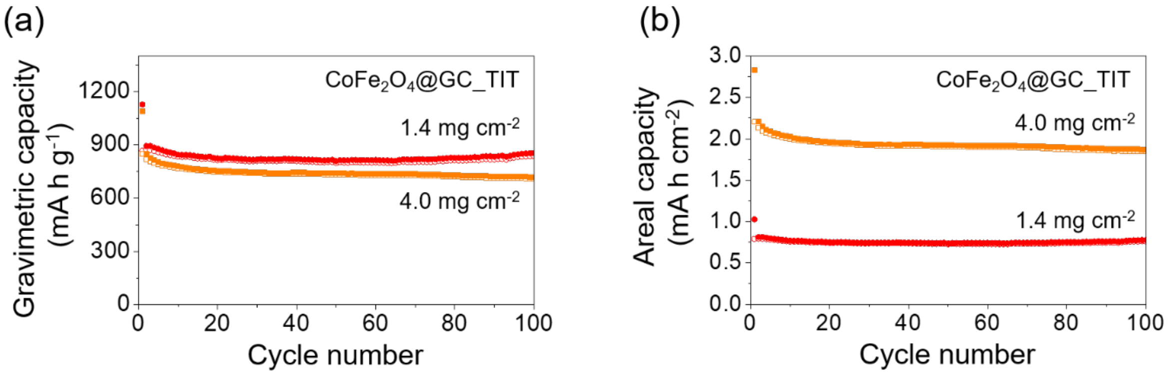

Fig. S10. (a) gravimetric and (b) areal capacities of $CoFe_2O_4$@GC_TIT with the different active materials mass loadings.

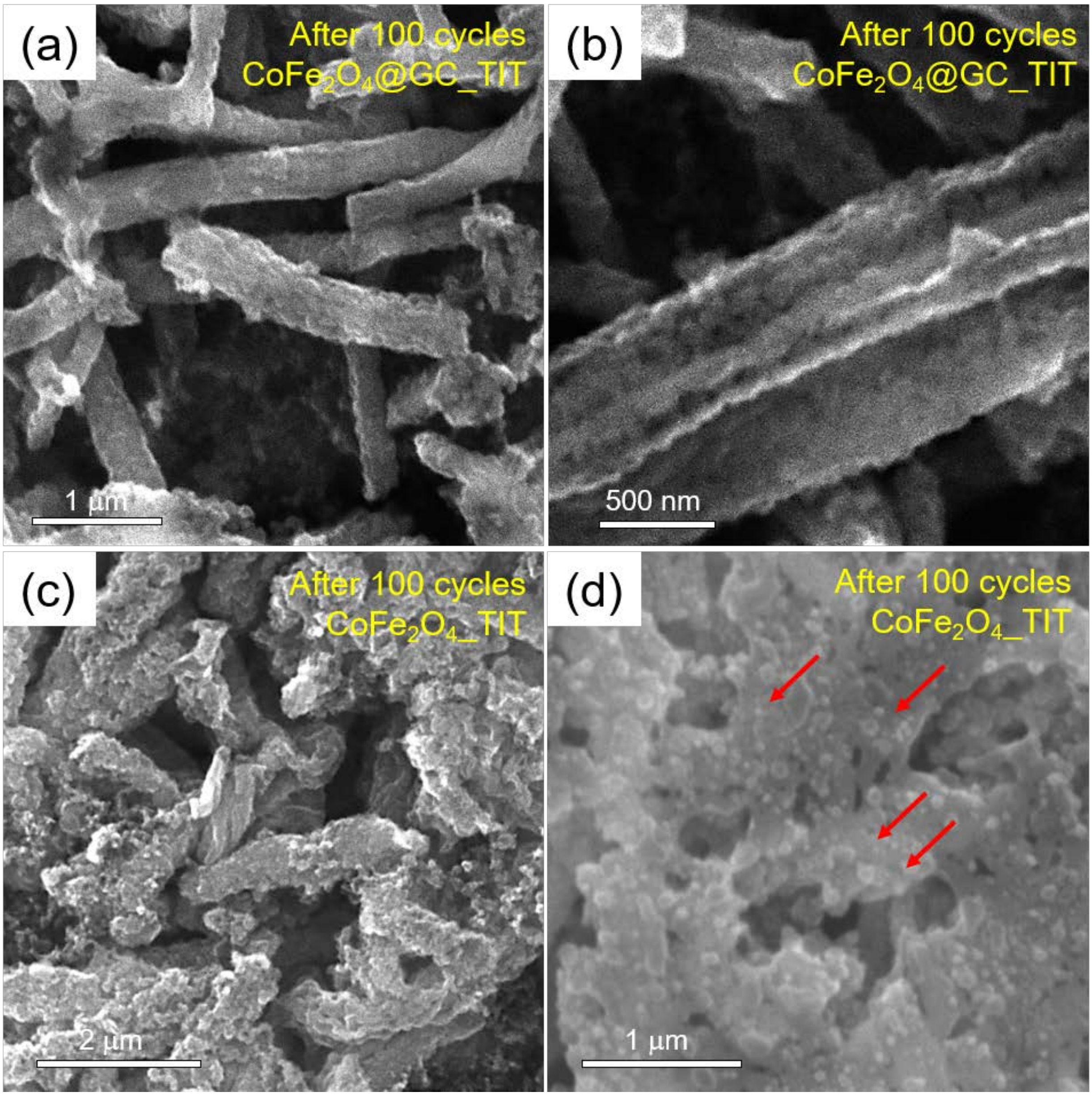

Fig. S11. Morphologies of $CoFe_2O_4$@GC_TIT and $CoFe_2O_4$_TIT after 100 cycling at a current density of 1.0 A g^{-1}.

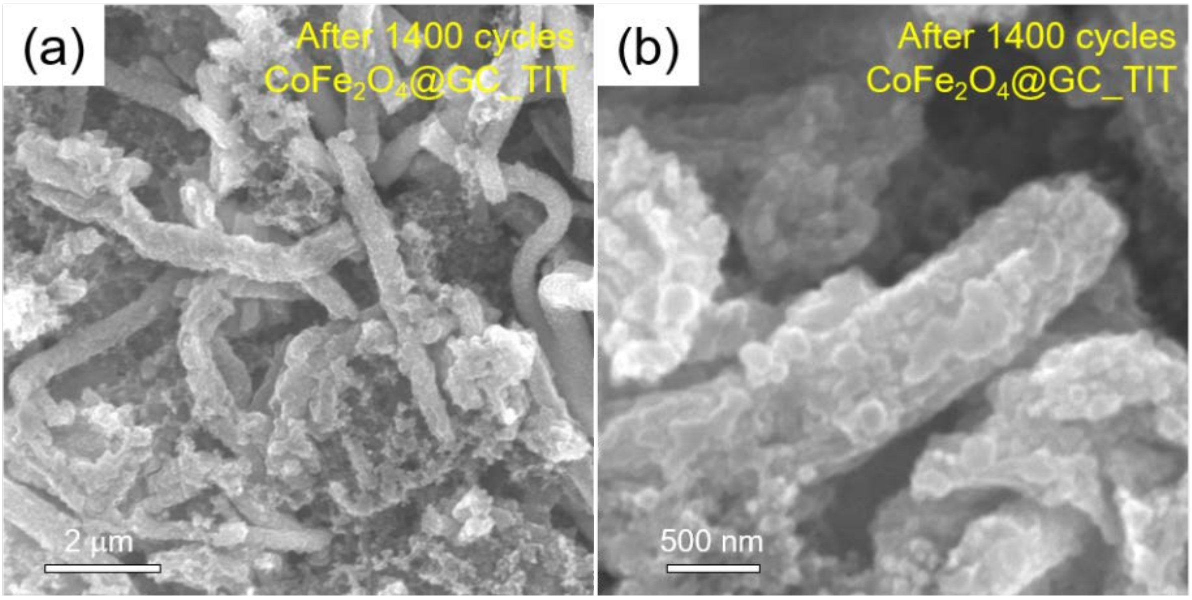

Fig. S12. SEM images of $CoFe_2O_4$@GC_TIT after 1400 cycles.

Table S1. Electrochemical properties of various cobalt and iron oxide electrode materials reported in the previous literature.

Materials	**Current rate**	**Discharge capacity [mA h g^{-1}] and (cycle number)**	**Rate capacity [mA h g^{-1}] (current rate)**	**Ref**
Co_3O_4-nanobubble decorated rGO sphere	2.0 A g^{-1}	1156 (200)	842 (10.0 A g^{-1})	[S1]
Graphene-wrapped mesoporous cobalt oxide hollow spheres	1.0 A g^{-1}	600 (500)	259 (5.0 A g^{-1})	[S2]
Cobalt oxide nanoparticles-embedded nitrogen-doped porous carbon nanofibers	1.0 A g^{-1}	984 (400)	802 (1.2 A g^{-1})	[S3]
CoO/Co_3O_4-graphene hybrids	1.0 A g^{-1}	670 (700)	455 (4.0 A g^{-1})	[S4]
Carbon-encapsulated Fe_3O_4 nanoparticles	5.0 A g^{-1}	836 (350)	297 (20.0 A g^{-1})	[S5]
N-doped dual carbon-confined 3D architecture rGO/Fe_3O_4/AC	5.0 A g^{-1}	~500 (500)	437 (10.0 A g^{-1})	[S6]
Pomegranate-like, carbon-coated Fe_3O_4	5.0 A g^{-1}	520 (1000)	416 (10.0 A g^{-1})	[S7]
Neuron-inspired Fe_3O_4-conductive carbon	1.0 A g^{-1}	971 (1000)	206 (8.0 A g^{-1})	[S8]
Macroporous Fe_3O_4@C	2.0 A g^{-1}	645 (1000)	300 (10.0 A g^{-1})	[S9]
C@$CoFe_2O_4$ fiber-in-tube mesoporous nanostructure	0.2 A g^{-1}	700 (150)	488 (1.6 A g^{-1})	[S10]
Core/shell structured $CoFe_2O_4$/onion-like C nanocapsules	0.1 A g^{-1}	914 (500)	617 (3.7 A g^{-1})	[S11]
Layer-stacked $CoFe_2O_4$ mesoporous platelets	5.0 A g^{-1}	580 (2000)	654 (10.0 A g^{-1})	[S12]
Tube-in-tube structured nanofibers comprising hollow $CoFe_2O_4$ nanospheres coated with GC layers	***3.0 A g^{-1}***	***682 (1400)***	***355 (50.0 A g^{-1})***	***In this work***

References

[S1] G.D. Park, J.S. Cho, Y.C. Kang, *Nano Energy*, 2015, **17**, 17-26.

[S2] H. Sun, X. Sun, T. Hu, M. Yu, F. Lu, J. Lian, *J. Phys. Chem. C*, 2014, **118**, 2263-2272.

[S3] X. Wang, Y. Tang, P. Shi, J. Fan, Q. Xu, Y. Min, *Chem. Eng. J.*, 2018, **334**, 1642-1649.

[S4] C. Hu, J. Yang, C. Yu, S. Li, Y. Mu, S. Bai, M. Wang, S. Liang, J. Qiu, *Chem. Eur. J.*, 2019, **25**, 5527-5533.

[S5] C. He, S. Wu, N. Zhao, C. Shi, E. Liu, J. Li, *ACS Nano*, 2013, **7**, 4459-4469.

[S6] R. Ding, J. Zhang, J. Qi, Z. Li, C. Wang, M. Chen, *ACS Appl. Mater. Interfaces*, 2018, **10**, 13470-13478.

[S7] D. Han, G. Guo, Y. Yan, T. Li, B. Wang, A. Dong, *Energy Storage Mater.*, 2018, **10**, 32-39.

[S8] S.-M. Hao, Q.-J. Li, J. Qu, F. An, Y.-J. Zhang, Z.-Z. Yu, *ACS Appl. Mater. Interfaces*, 2018, **10**, 17923-17932.

[S9] Z. Yan, X. Jiang, Y. Dai, W. Xiao, X. Li, N. Du, G. He, *ACS Appl. Mater. Interfaces*, 2018, **10**, 2581-2590.

[S10] J. Wang, G. Yang, L. Wang, W. Yan, W. Wei, *J. Alloys Compd.*, 2017, **693**, 110-117.

[S11] X. Liu, N. Wu, C. Cui, P. Zhou, Y. Sun, *J. Alloys Compd.*, 2015, **664**, 59-65.

[S12] Z. Zhang, W. Li, R. Zou, W. Kang, Y. S. Chui, M. F. Yuen, C.-S. Lee, W. Zhang, *J. Mater. Chem. A*, 2015, **3**, 6990-6997.